Available online at www.sciencedirect.com

ScienceDirect

Procedia CIRP 118 (2023) 402–407

www.elsevier.com/locate/procedia

16th CIRP Conference on Intelligent Computation in Manufacturing Engineering, CIRP ICME '22, Italy

Modelling of micro-milling by considering tool run-out and ploughing regime

Cristian Cappellini[a,*], Andrea Abeni[b], Aldo Attanasio[b]

[a]*Faculty of Science and Technology, Free University of Bolzano, P.zza Università 5, Bolzano, 39100, Italy*

[b]*University of Brescia, Department of Mechanical and Industrial Engineering, V. Branze 38, Brescia 25123, Italy*

* Corresponding author. Tel.: +39-+39-0471-017114; *E-mail address:* cristian.cappellini@unibz.it

Abstract

The accuracy in micro-milling is strongly affected by the phenomena of tool run-out. The discordance between the tool edge effective and theoretical trajectories increases the tool wear and it negatively affects the quality of the machined surface. The tool run-out should be considered in machining modelling in order to accurately predict how the cutting force changes as the process parameters change. This paper describes the structure of an analytical model which computes the cutting force by considering the tool run-out and the concurrent presence of ploughing- and shearing- dominated cutting regimes. The model was finally calibrated by considering micro-machining on difficult-to-cut material.

© 2023 The Authors. Published by Elsevier B.V.
This is an open access article under the CC BY-NC-ND license (https://creativecommons.org/licenses/by-nc-nd/4.0)
Peer-review under responsibility of the scientific committee of the 16th CIRP Conference on Intelligent Computation in Manufacturing Engineering

Keywords: Tool run-out; Micro-milling; Analytical Model

1. Introduction

The designation of micro-machining indicates machining operation performed by using tools with diameters typically smaller than one millimeter and edge roundness size equal to few micrometers [1]. Negative rake angles resulted as an effect of the comparability between the chip thickness and the edge roundness [2]. The analytical or numerical modeling of the process must take account of this peculiarity and the models commonly utilized in conventional scale machining cannot be utilized to correctly predict the cutting force in micro-machining. An effective model must consider the coexistence of shearing cutting regime with ploughing [3, 4], which determines higher than expected cutting force and poor surface finishing. Among the analytical models suitable for micro milling [5–7], only few of them considers ploughing effect combined with tool run-out.

Tool run-out phenomena is considered one of the most meaningful issues which affects quality of the machined parts and repeatability of micro-milling process. It consists in a deviation of the cutting edge actual trajectories from the cycloid path that should be theoretically followed by each cutting edge during tool rotation. The tool run-out effect determines different trajectories for each cutting edge of an end-mill and furthermore it has a meaningful effect on the uncut chip thickness value. A correct modeling of tool run-out is crucial to compute the actual chip section and the cutting regime as a consequence. Different researchers tackled the issue of the tool run-out modeling by developing geometrical and analytical models [8, 9] or by performing numerical investigation and FEM simulations [10, 11]. This research introduces the utilization of a new analytical model which can consider ploughing and tool run-out effect both. The model was calibrated on the data collected during experimental tests conducted on samples in Ti6Al4V (Ti64) titanium alloy manufactured by Laser-Based Powder Bed Fusion (PBF-LB) by using micro-mills with a nominal diameter of 0.5 mm and two flutes. During the micro-machining, the cutting forces were measured by using a triaxial loadcell in order to compare the experimental data with the asymmetric cutting force predicted by the model. The tool run-out phenomena were described by some geometrical parameters which can be experimentally estimated by considering the periodicity of the cutting force signal and the morphology of the machined samples.

2212-8271 © 2023 The Authors. Published by Elsevier B.V.
This is an open access article under the CC BY-NC-ND license (https://creativecommons.org/licenses/by-nc-nd/4.0)
Peer-review under responsibility of the scientific committee of the 16th CIRP Conference on Intelligent Computation in Manufacturing Engineering
10.1016/j.procir.2023.06.069

2. Materials and Methods

2.1. Mechanistic modeling of cutting forces with tool run-out

Tool run-out is defined as the deviation of the theoretical tool rotational axis from the physical actual one. In conventional milling operations the effect of tool run-out can be considered negligible, but in micro-milling processes, due to the extreme precision required by the machining process, it cannot be neglected, and its analysis is mandatory to achieve the expected reliable quality. Tool run-out can be defined by the run-out length r_0 and the run-out angle γ, as shown in Figure 1, representing the topology of tool run-out for a two flute micro-mill, on a plane normal to the tool rotational axis.

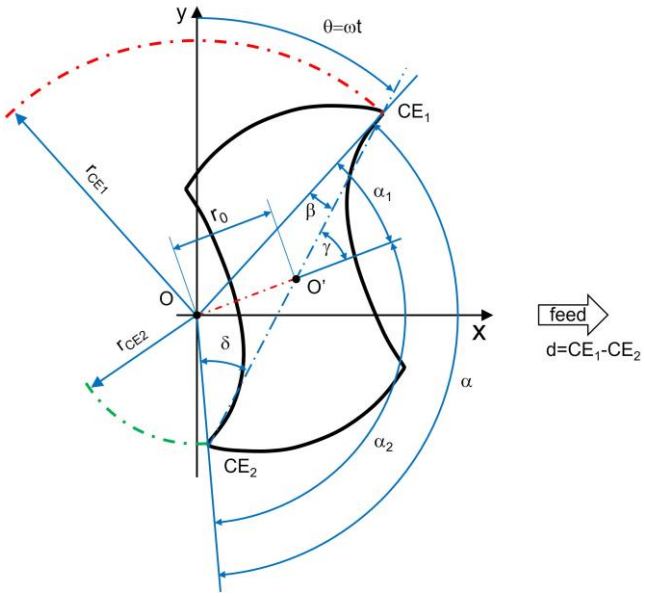

Fig. 1. Geometrical representation of tool run-out.

In presence of tool run-out, the phase angle α between the mill cutting edges (CE_i), and the cutting edge radii r_{CEi} are functions of r_0 and γ parameters. It has been demonstrated in [12] that, once the radius of the first cutting edge r_{CE1}, α, and tool diameter d, are known, it is possible to evaluate all the geometrical parameters. This assessment permits to estimate the chip cross-sectional area evolution, on which the proposed micro-milling tool force model is based, hence it is of fundamental importance for its development. Considering Figure 1, the tool rotational angle $\theta(t)$ is defined in Eq. (1):

$$\theta(t) = \omega \cdot t \tag{1}$$

where ω is the tool rotational speed [rad/s] and t is the cutting time [s]. The cutting edges trajectories are expressed by their components on x-axis and y-axis by Eq. (2):

$$\begin{aligned} x_{CE1} &= r_{CE1} \cdot \sin\theta + \frac{f}{60} \cdot t \\ y_{CE1} &= r_{CE1} \cdot \cos\theta \\ x_{CE2} &= r_{CE2} \cdot \sin[\theta + \alpha] + \frac{f}{60} \cdot t \\ y_{CE2} &= r_{CE2} \cdot \cos[\theta + \alpha] \end{aligned} \tag{2}$$

where f is the feed [mm/min] and r_{CE2} is the CE_2 radius [mm] calculated by Equations (3) and (4) respectively:

$$r_{CE2} = \sqrt{r_{CE1}^2 + d^2 - 2 r_{CE1} d \cos\beta} \tag{3}$$

$$f = f_Z \cdot z \cdot N \tag{4}$$

With f_Z is the feed per tooth [mm/tooth/rev], z the number of flutes of the mill, and N the spindle speed [rpm].

Once the temporal trajectories of $CE_1(x_{CE1},y_{CE1})$ and $CE_2(x_{CE2},y_{CE2})$ are derived, the calculation of the instantaneous uncut chip thickness (IUCT) for each one of them is obtained by their difference, leading to Eq. (5) for IUCT of CE_1 (h_{CE1}) and CE_2 (h_{CE2}):

$$\begin{aligned} h_{CE1} &= \sqrt{(r_{CE1}\sin\theta + \Delta s_{CE1})^2 + (r_{CE1}\cos\theta)^2} - r_{CE2} \\ h_{CE2} &= \sqrt{(r_{CE2}\sin\theta + \Delta s_{CE2})^2 + (r_{CE2}\cos\theta)^2} - r_{CE1} \end{aligned} \tag{5}$$

Where Δs_{CE1} is the distance covered by the rotational axis between the passage of CE_2 and the consecutive passage of CE_1 in the θ angular position, while Δs_{CE2} is the distance covered between the passage of CE_1 and the consecutive passage of CE_2 in the θ angular position. These distances are evaluated by Eq. (6):

$$\begin{aligned} \Delta s_{CE1} &= \frac{f}{60} \cdot \frac{\alpha}{\omega} \\ \Delta s_{CE2} &= \frac{f}{60} \cdot \frac{2\pi - \alpha}{\omega} \end{aligned} \tag{6}$$

As understandable from Eq. (5) and from Figure 2, tool run-out leads to a difference amongst the IUCT of first and second cutting edge. Therefore, the related cutting forces will be different as well. The proposed model deals not only with the tool run-out effect, but also with the contribution of shearing and ploughing cutting regimes to the generated forces. Thus, detecting the transition between ploughing and shearing regimes, and calculating the cutting area A_C covered by each cutting edge is mandatory. Figure 2 reports the schematization of the cutting edges trajectories in presence of tool run-out and the cutting force components in a plane normal to the tool rotational axis.

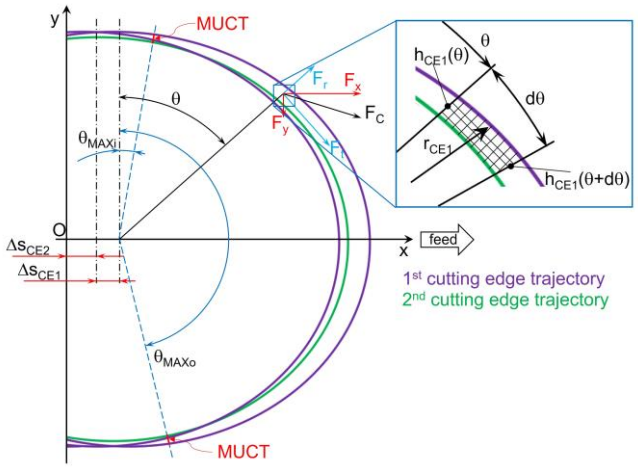

Fig. 2. Trajectories and cutting forces for micro-milling operation.

The cutting area of the i-th cutting edge can be estimated by Eq. (7)

$$A_{ci}(\theta) = \int_0^{\theta} \left(\frac{h_{CEi}(\theta)+h_{CEi}(\theta+d\theta)}{2}\right) r_{CEi}\, d\theta \quad (7)$$

where $d\theta$ is the infinitesimal variation of the rotational angle.

The transition between ploughing and shearing cutting regimes is detected by the value of the minimum uncut chip thickness (MUCT), related to cutting edge radius and workpiece material, and must be experimentally determined (Section 2.2).

The total cutting force F_C is the combination of its three axial components F_x, F_y, and F_z (this last not visible in Figure 2), and the resulting one in the plane can be subdivided in its tangential F_t and radial F_r components. These latter can be expressed by Eq. (8):

$$\begin{aligned} F_{t1} &= \left(K_{ts} \cdot h_{CE1}(\theta) + K_{tp} \cdot A_{pCE1}(\theta)\right) \cdot a_p \\ F_{r1} &= \left(K_{rs} \cdot h_{CE1}(\theta) + K_{rp} \cdot A_{pCE1}(\theta)\right) \cdot a_p \\ F_{t2} &= \left(K_{ts} \cdot h_{CE2}(\theta) + K_{tp} \cdot A_{pCE2}(\theta)\right) \cdot a_p \\ F_{r2} &= \left(K_{rs} \cdot h_{CE2}(\theta) + K_{rp} \cdot A_{pCE2}(\theta)\right) \cdot a_p \end{aligned} \quad (8)$$

Where K_{ts} and K_{rs} are the specific force coefficients [N/mm^2] for the shearing regime, K_{tp} and K_{rp} are the specific force coefficients [N/mm^3] for the ploughing regime, a_p [mm] is the axial depth of cut, and $A_{pCE}(\theta)$ is the ploughed area [mm^2].

Once MUCT is individuated, $A_{pCE}(\theta)$ can be assessed applying the set of Eq. (9):

$$\begin{aligned} h_{CEi}(\theta) < MUCT \wedge \theta < \theta_{MAXi} \quad &\Rightarrow \quad A_{pCEi}(\theta) = A_{ci}(\theta) \\ hCEi(\theta) > MUCT \quad &\Rightarrow \quad A_{pi}(\theta) = A_{piMAX} \\ h_{CEi}(\theta) < MUCT \wedge \theta > \theta_{MAXo} \quad &\Rightarrow \quad A_{pCEi}(\theta) = A_{ci}(\pi) - A_{ci}(\theta) \end{aligned} \quad (9)$$

Where θ_{MAXi} is the tool rotational angle at which IUCT reaches the value of MUCT in the entering phase, and θ_{MAXo} is the tool rotational angle at which the IUCT becomes smaller than MUCT in the exiting phase.

The aim of this paper is to calibrate K_{ts}, K_{rs}, K_{tp}, and K_{rp} for correctly forecasting the cutting force components.

2.2. Experimental setup

In order to acquire the micro-milling force components, necessary for the calibration and validation of the proposed model, an extensive experimental campaign has been performed. The micro-milled specimens were realized by Powder Bed Fusion (PBF) additive manufacturing process, by Selective Laser Melting (SLM) of Ti6Al4V powders, namely EOS Ti6Al4V with an EOS M290. As stated by the datasheet, in accordance with ASTM B214, B15, B212, F2924 and F1472 standards [13, 14], Table 1 reports chemical composition and properties of the employed powders.

Table 1. Properties of the Ti6Al4V employed powders.

Element	Chem. Comp. [%wt]
Al	5.92
V	4.04
O	0.13
Fe	0.20
Ti	Balance
Particle size [µm]	
d10	27.79
d50	31.18
d90	54.45
Powder apparent density [g/cm^3]	2.31

The specimens were built with a cubic geometry with an edge length of 10 mm, and with a growing angle respect to the building plate of 0°. The angle between each layer was of 67°. The SLM process parameters were a laser power of 340 W, a laser focus of 70 µm, a scanning speed of 1250 mm/s, a hatch spacing of 40 µm, and a slice thickness of 30 µm. Support structures for enhancing SLM process stability were realized applying a laser power of 100 W and a scanning speed of 600 mm/s. The whole additive manufacturing process was performed in a controlled argon gas atmosphere for preventing oxygen contamination. The supports were then removed, and the specimens were sonically cleaned in an acetone-isopropanol solution. The micro-milling tests were performed by a five axis nano-precision machining center KERN Pyramid Nano equipped with a Heidenhain iTCN 530 numeric control. The force components measurement was achieved by a loadcell Kistler 9317C cabled with a Kistler 5015A amplifier [15]. To prepare a flat surface on the specimens, a roughing pass by a three-flutes bottom mill with a diameter of 3 mm, a depth of cut of 100 µm, a cutting speed of 100 m/min, and a feed of 7.5 µm/tooth was carried out. After this, the tests of microchannels machining were accomplished by a two-flutes micro-mill (Table 2) in dry conditions, as suggested by the tool manufacturer in case of Ti6Al4V cutting by Titanium Nitride coated tools. The optical measurements of micro-channels' widths were then accomplished by a Hirox RH 2000 confocal microscope.

Table 2. Properties of the tool employed for micro-channels machining.

Property	Value
Model	Rime HM79/05
Nom. diam. [µm]	500
Eff. diam. [µm]	475 ±4
Helix angle [°]	30
Material	Tungsten Carbide
Coating	Titanium Nitride

The totality of the cutting tests was exploited for detecting the tool run-out parameters, and for calibrating the cutting force model. Eight micro-channels were machined maintaining a constant cutting speed V_C = 40 m/min, a constant axial depth of cut a_p = 0.05 mm, and varying the feed per tooth f_Z at regular interval in a range between 0.75 ÷ 4.0 µm/tooth. The upper limit of 4.0 µm/tooth was experimentally selected after

detecting that, at $f_Z = 5.0$ µm, a catastrophic tool breakage occurred. For each executed test, F_C was calculated as the vectorial sum of the three acquired force components F_x, F_y, F_z, and the related specific cutting force (*SCF*), expressed in [N/mm^2] was derived by Eq. (10):

$$SCF(\theta) = \frac{F_C(\theta)}{a_p \cdot h_{CEi}(\theta)} = \frac{F_C(\theta)}{a_p \cdot f_Z \cdot \sin(\theta)} \quad (10)$$

The *SCF* peak for every test was plotted as a function of f_Z (Figure 3) and used for MUCT assessment.

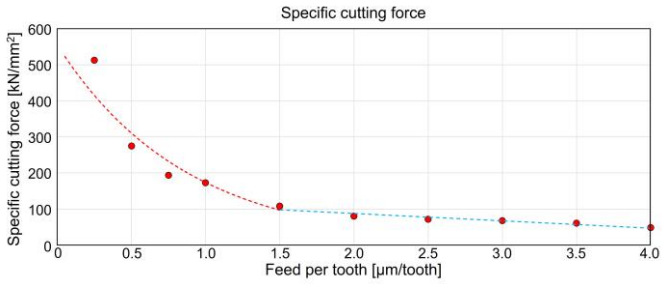

Fig. 3. Specific Cutting Force value as function of feed per tooth.

Figure 3 shows that at low f_Z values, here only ploughing regime is present, *SCF* rapidly decreases, while at f_Z values higher than 1.5 µm, *SCF* is stabilized. As reported in [16], a MUCT = 1.5 µm has been selected.

As previously reported, the evaluation of r_0 and γ concerns the estimation of d, r_{CE1}, and α. The value of the effective tool diameter was measured by the BLUM laser measuring system mounted on the CNC machine (Table 2). As reported in [12], r_{CE1} was derived by halving the measurements of the machined micro-channels widths (Figure 4), while α was detected, by analyzing the acquired force signal as a function of the rotational angle of the tool, and evaluating the angle between the F_C local minima, that indicates the transition amongst one cutting edge and the other (Figure 5).

Fig. 4. Experimental measurement of r_{CE1}.

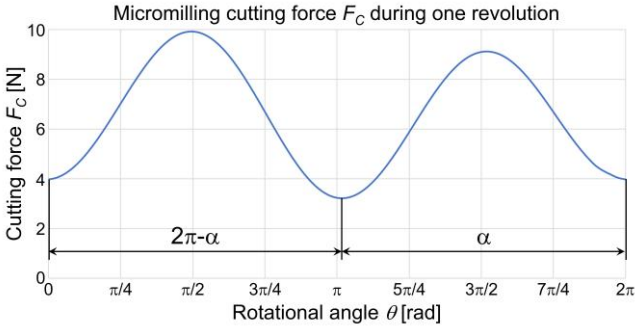

Fig. 5. Phase angle α [rad] measurement from the acquired force signal.

2.3. Force model coefficients optimization

The optimization of the model coefficients K_{ts}, K_{rs}, K_{tp}, K_{rp} (Eq. (8)) was attained employing the Particle Swarm Optimization (PSO) algorithm by Eberhart and Kennedy [17], whose use was proven in several applications [18, 19]. The error function to be minimized (Eq. (11)) was the normalized difference between the model peak force and the peak of the experimental one for each cutting edge and each performed test:

$$Err = \sum_{i,j} \left(\frac{|F_{C,modMAX,CEi} - F_{C,expMAX,CEi}|}{F_{C,expMAX,CEi}} \right)_j \quad \begin{matrix} i = 1,2 \\ j = 1 \div 10 \end{matrix} \quad (11)$$

where the i and j indexes indicate the cutting edge number and the test number respectively.

For the evaluation of the forces and of the function *Err*, the Eqs. from (1) to (11) of the analytical model were implemented in a Matlab® function. By applying on it the PSO search algorithm, *Err* was iteratively minimized, permitting the calibration of K_{ts}, K_{rs}, K_{tp}, K_{rp} coefficients. An initial assumption of these latter led to a first *Err* estimation by the comparison with experimental data. Subsequently, the algorithm iteratively adjusted the coefficients by respecting the constraints related to their modification, until achieving the *Err* minimized value. This process concerned a domain for K_{ts} and K_{rs} of [0;100000], while a domain for K_{tp} and K_{rp} of [0;1000000]. A population number of 100 particles and an iteration number of 1000 was set for the PSO algorithm. In order to attain a more accurate solution, the PSO was executed ten times.

3. Results and Discussion

Amongst all the iterations performed by the applied PSO algorithm, the one furnishing the best result provides the lowest value of *Err* equal to 4.187. The resulting calibrated coefficients result to be: $K_{ts} = 99521$ N/mm^2, $K_{rs} = 4723$ N/mm^3, $K_{tp} = 259364$ N/mm^2, and $K_{rp} = 27275$ N/mm^3.

Table 3 reports the percentage errors for each performed test and for each cutting edge. The error $e_{\%}$ is calculated by Eq. (12):

$$e_{\%} = \frac{|F_{C,modMAX,CEi} - F_{C,expMAX,CEi}|}{F_{C,expMAX,CEi}} \cdot 100 \quad (12)$$

Where, also in this case, the i-index indicates the i-th cutting edge.

Table 3. Percentage error $e_{\%}$ for each performed test and cutting edge.

First cutting edge (CE_1)		Second cutting edge (CE_2)	
f_Z [µm/tooth]	$e_{\%}$	f_Z [µm/tooth]	$e_{\%}$
4.0	0.32	4.0	3.03
3.5	13.98	3.5	9.60
3.0	20.34	3.0	22.22
2.5	4.93	2.5	8.39
2.0	7.13	2.0	6.13
1.5	30.01	1.5	75.55
1.0	0.16	1.0	24.80
0.75	12.18	0.75	22.97

Figures from 6 to 13 report the evolution of the experimental and modeled cutting forces as a function of the rotational angle of the tool. These figures show the capability of the proposed model to correctly estimate the asymmetric behavior of the forces as a consequence of the tool run-out. More in detail, the model correctly forecast the phase angle between the first and the second cutting edge, and it is able to predict which one, amongst these two, will generate the higher cutting force and which one the lower.

The precision of the model is higher at higher feed per tooth, in a range of f_Z values from 4.0 µm to 2.0 µm, and this is noticeable by observing Table 3 as well. For f_Z values lower than 2.0µm, $e_{\%}$ increases up to a value of 75.55 %, for the second cutting edge, when f_Z is equal to 1.5 µm, that is the value indicating the transition between ploughing and shearing cutting regime. This behavior is ascribable to the increment of ploughing regime contribution. In these circumstances in fact, the machined material is mainly deformed instead of being sheared, leading to a more discontinuous cross-sectional area of the chip, that makes difficult its correct calculation by the analytical geometrical model. For all the other values of f_Z, $e_{\%}$ is lower than the 25 %, indicating the capability of the analytical model to calculate the cutting forces in a suitable way. Therefore, the proposed technique can be profitably employed for considering the presence of tool run-out in the prediction of micro-milling cutting forces.

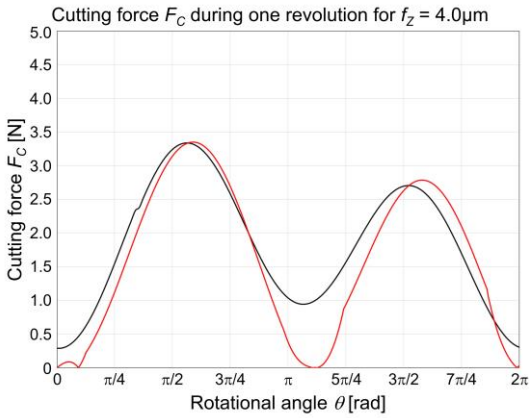

Fig. 6. Experimental vs. modeled F_C for f_Z = 4.0 µm.

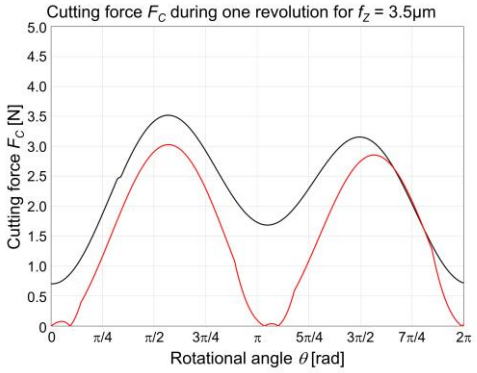

Fig. 7. Experimental vs. modeled F_C for f_Z = 3.5 µm.

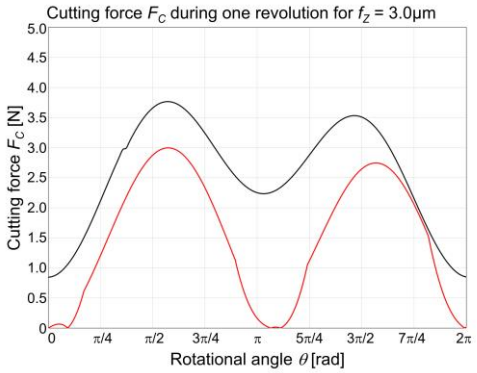

Fig. 8. Experimental vs. modeled F_C for f_Z = 3.0 µm.

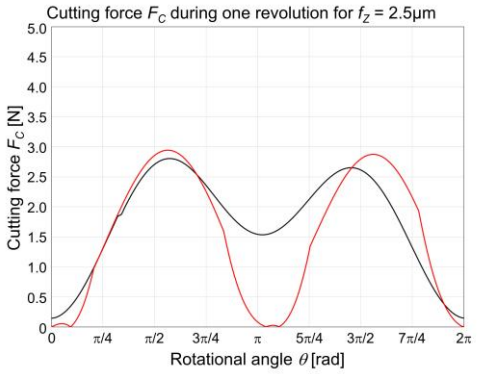

Fig. 9. Experimental vs. modeled F_C for f_Z = 2.5 µm.

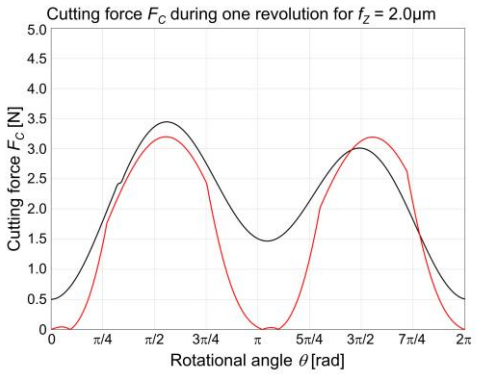

Fig. 10. Experimental vs. modeled F_C for f_Z = 2.0 µm.

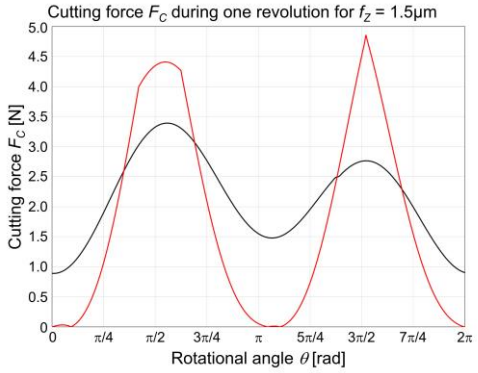

Fig. 11. Experimental vs. modeled F_C for f_Z = 1.5 µm.

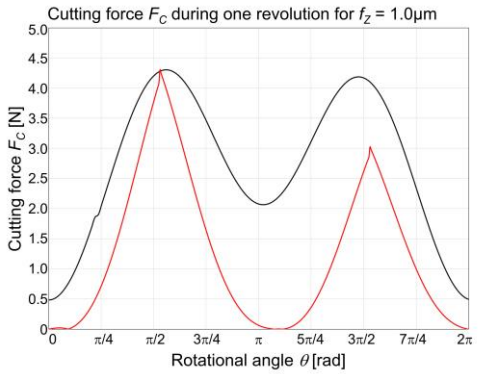

Fig. 12. Experimental vs. modeled F_C for f_Z = 1.0 µm.

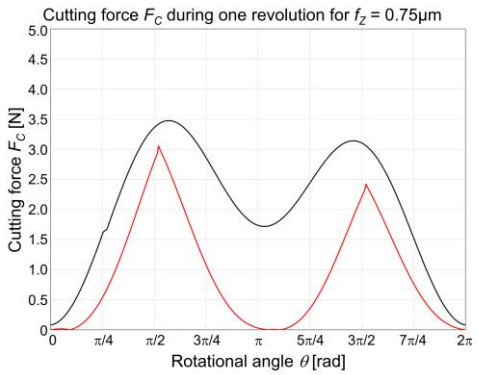

Fig. 13. Experimental vs. modeled F_C for f_Z = 0.75 µm.

4. Conclusions

In this work, an analytical model considering the transition between ploughing and shearing regime in cutting, and the effects of tool run-out for the evaluation of the asymmetrical behavior of machining forces in micro-milling operations, is presented. The proposed model concerns the topology evolution of the cross-sectional area of the chip, and the optimization of dedicated cutting coefficients for ploughing and shearing contributions. The detection of these latter was achieved minimizing the difference in the comparison of experimental cutting forces, acquired during an extensive machining campaign of Ti6Al4V and the forces estimated by the analytical model, by the application of a PSO algorithm. The modeled forces result to be in good agreement with the experimental ones, underlining the reliability of the proposed methodology. In this manner, once that the tool run-out parameters and the MUCT value are known, it is possible to exploit the analytical model for predicting the micro-milling forces, avoiding the need of expensive and time-consuming experimental tests.

References

[1] O'Toole L, Kang CW, Fang FZ. Precision micro-milling process: state of the art. Adv Manuf 2021;9(2):173-205.
[2] Aslantas K, Alatrushi LKH. Experimental study on the effect of cutting tool geometry in micro-milling of Inconel 718. Arabian J Sci Eng 2021;46(3):2327-2342.
[3] Wojciechowski S. Estimation of Minimum Uncut Chip Thickness during Precision and Micro-Machining Processes of Various Materials—A Critical Review. Materials 2021;15(1):59.
[4] Balázs BZ, Geier N, Takács M, Davim JP. A review on micro-milling: recent advances and future trends. Int J Adv Manuf Technol 2021;112(3):655-684.
[5] Zhou L, Peng FY, Yana R, Yao PF, Yang CC, Li B. Analytical modeling and experimental validation of micro end-milling cutting forces considering edge radius and material strengthening effects. Int J Mach Tools Manuf 2015;97:29–41
[6] Zhang X, Ehmann KF, Yu T, Wang W. Cutting forces in micro-end-milling processes. Int J Mach Tools Manuf 12016;07:21–40
[7] Abeni A, Loda D, Özel T, Attanasio A. Analytical force modelling for micro milling additively fabricated Inconel 625. Prod Eng 2020;14(5-6):613-627.
[8] Li G, Li S, Zhu K. Micro-milling force modeling with tool wear and runout effect by spatial analytic geometry. Int J Adv Manuf Technol 2020;107(1):631-643.
[9] Jing X, Lv R, Song B, Xu J, Jaffery SHI, Li H. A novel run-out model based on spatial tool position for micro-milling force prediction. J Manuf Process 2021;68:739-749.
[10] Abeni A, Elisabetta C, Tugrul Ö, Aldo A. FEM simulation of micromilling of CuZn37 brass considering tool run-out. Proc CIRP 2019;82:172-177.
[11] Jing X, Lv R, Chen Y, Tian Y, Li H. Modelling and experimental analysis of the effects of run out, minimum chip thickness and elastic recovery on the cutting force in micro-end-milling. Int J Mech Sci 2020;176:105540.
[12] Attanasio A. Tool run-out measurement in micro milling. Micromachines 2017;8:221.
[13] ASTM B214-16 Standard Test Method for Sieve Analysis of Metal Powders ASTM: West Conshohocken, PA, USA, 2016; Volume 02.05 .
[14] ASTM F2924-14 Standard Specification for Additive Manufacturing Titanium-6 Aluminum-4 Vanadium with Powder Bed Fusion ASTM: West Conshohocken, PA, USA, 2014; Volume 10.04.
[15] Abeni A, Metelli A, Cappellini C, Attanasio A. Experimental Optimization of Process Parameters in CuNi18Zn20 Micromachining. Micromachines 2021;12(11):1293.
[16] Abeni A, Ginestra PS, Attanasio A. Comparison Between Micro Machining of Additively Manufactured and Conventionally Formed Samples of Ti6Al4V Alloy. In: Ceretti E, Tollio T, editors. Selected Topics in Manufacturing. Cham: Springer; 2022. p. 91-106.
[17] Eberhart R, Kennedy J. A new optimizer using particle swarm theory. In: Proceedings of the Sixth International Symposium on Micro Machine and Human Science. Nagoja: IEEE; 1995. p. 39-43.
[18] Raja SB, Baskar N. Particle swarm optimization technique for determining optimal machining parameters of different work piece materials in turning operations. Int J. Adv Manuf Technol 2011;54(5-8):445-463.
[19] Ciurana J, Arias G, Özel T. Neural network modeling and particle swarm optimization (PSO) of process parameters in pulsed laser micromachining of hardenend AISI H13 steel. Mater Manuf Process 2009;24(3):358-368.